UNIVERSITY *of* York

This is a repository copy of *Morphological study on human body absorption cross section in a reverberation chamber from 1 GHz to 16 GHz*.

White Rose Research Online URL for this paper:
https://eprints.whiterose.ac.uk/141345/

Version: Accepted Version

Article:

White Rose
university consortium
Universities of Leeds, Sheffield & York

eprints@whiterose.ac.uk
https://eprints.whiterose.ac.uk/

Morphological study on human body absorption cross section in a reverberation chamber from 1 GHz to 16 GHz

Xiaotian Zhang, Martin Robinson, Ian Flintoft, John Dawson, Sarah Parker

Abstract—**The human body absorption cross section (ACS) is important in non-ionizing radiation dosimetry, but it is always hard to accurately evaluate the ACS of an individual from his or her morphological parameters, such as height and weight. To obtain an empirical formula that can evaluate the ACS from morphological parameters, 48 subjects with different morphological parameters were measured from 1 GHz to 16 GHz in a reverberation chamber. The ACS was extracted from the power delay profile (PDP). This has the advantage of not requiring antenna radiation efficiency, and it has not been used in a wide-band group study like this before. The accuracy of the ACS measurement is demonstrated by comparision with the ACS of a spherical model with known structure and material, and the mean absolute percentage error (MAPE) of the sphere measurement is just 3.4%. Statistical analsysis shows that the body surface area (BSA) has the strongest correlation with the ACS amongst all the morphological parameters, therefore we present a new empirical ACS formula as a function of BSA and frequency. This will be of interest to those considering dosimetry, and in computing the effect of human body absorption on radio propagation in vehicles and other structures.**

Index Terms—**absorption cross section, anthropometry, inverse Fourier transforms, reverberation chambers, nonionized dosimetry**

I. INTRODUCTION

The absorption cross section (ACS) of an object is its equivalent area for collecting electromagnetic (EM) power from incident waves. Knowledge of the human body ACS is of fundamental importance in many applications, such as non-ionizing radiation dosimetry, indoor radio channel modelling, determining the interference between onboard electronic systems, etc. [1], [2], [3]. In the indoor multipath environment, the power delay spread relies heavily on the properties and numbers of absorbing objects presented in the room. Since the human body is a lossy object, its influence on the power delay spread can not be neglected [1]. Formulas showing the relations of the power delay spread to the ACS are given in [4]. This paper will focus on the ACS of the human body in a diffuse (reverberant) EM environment. For simplicity, all the ACS values mentioned in this paper are the averaged ACS in diffuse field, unless otherwise stated.

The accurate determination of human body ACS is not easy. It either requires expensive measurement instruments or significant computational power, which is only found in specialised facilities. For general researchers, a simple method of quickly estimating human body ACS is desireable.

The aim of this research was to find an empirical formula by which the human body ACS can be quickly evaluated from morphological parameters, such as height, weight, body fat percentage (BFP), etc. In order to obtain such a formula, 48 volunteers of different morphological types were recruited and their ACS values were measured from 1 GHz to 16 GHz in a reverberation chamber (RC).

There has been some previous research on the measurement of human body ACS in diffuse environments, but due to the complexity of the problem, they are not usually thorough enough, and accurate wide-band group studies are scarce. Melia et al. measured the ACS values of 60 adults in a RC, but the ACS was determined from the net power transfer function between two antennas which relies on knowledge of the antenna radiation efficiency [5], [6] , and that is generally not well known for most antennas. Bamba et al. determined the ACS from the power delay profile (PDP) which, does not require knowledge of the antenna radiation efficiency, but the measurement was only performed on one subject at a single frequency [2]. The wideband measurement of human body has been performed by Senić from 1 GHz to 8 GHz, but also on one subject [7], [8].

Since the measurement of the PDP does not require knowledge of the antenna radiation efficiency, all the ACS values in this work are determined from the PDP. The PDP is extracted from the inverse fast Fourier transform (IFFT) of the S_{21} measured in the frequency domain, by a vector network analyzer (VNA). This method can give accurate ACS results even without the calibration of VNA [9].

The remainder of this paper is organized as follows: Section II-A is a review on the theory and data processing techniques in the ACS measurement; Section II-B demonstrates the accuracy of the ACS measurement; Section II-C shows the posture's effect on the human body ACS; Section II-D gives the method of measuring morphological parameters; Discussions on the group measurement of human body ACS are given in Section III and the empirical formula for evaluating human body ACS is also given in this section.

II. MEASURING THE HUMAN BODY ACS IN AN RC

A. Methods of measuring human body ACS in an RC

Reverberation chamber theory is decribed in detail by Hill [10]. The important feature for this work is that an object placed in a reverberation chamber is illuminated equally with waves from all directions and of all polarisations with equal probability, when measurements are averaged over a number of stirrer positions and/or frequencies. The ACS in an RC can

be determined from the chamber quality factor, defined as [11], [12]:

$$< Q >= \omega \frac{< E >}{< P_d >}, \qquad (1)$$

where Q is the chamber quality factor, $< \cdot >$ means averaging over different stirrer positions; ω is angular frequency; E is the EM energy stored in the RC; P_d is the power dissipated in the RC. If a lossy object with large ACS is placed in an RC, P_d will increase which makes the Q factor become smaller. Therefore the ACS of an object placed in an RC can be obtained by measuring the change of the Q factor [11], [12]:

$$< \sigma_{\mathrm{a}} >= \frac{2\pi V}{\lambda} \left(\frac{1}{< Q_{\mathrm{wo}} >} - \frac{1}{< Q_{\mathrm{no}} >} \right), \qquad (2)$$

where $< \sigma_{\mathrm{a}} >$ is the average ACS of the object over all directions and polarisations; V is the volume of the RC; λ is the wavelength; Q_{wo} is the Q factor of the RC with the lossy object; Q_{no} is the Q factor of the RC without the lossy object present.

The Q factor of an RC can be determined in two different ways. The first way is to extract the Q factor directly from the S-parameters measured at the ports of two antennas loaded in the chamber. The Q factor can be evaluated from the S-parameters as [13], [12]:

$$< Q >= \frac{16\pi^2 V}{\lambda^3} \frac{< |S_{21}|^2 >}{(1 - | < S_{11} > |^2)(1 - | < S_{22} > |^2)\eta_{\mathrm{Tx}}\eta_{\mathrm{Rx}}}, \qquad (3)$$

where η_{Tx} and η_{Rx} are the radiation efficiencies of the transmitting antenna and receiving antenna. Determining the Q factor using (3) requires η_{Tx} and η_{Rx} to be known.

This problem can be solved by determining the Q factor in the second way, where it is calculated from the chamber power decay time constant τ [10]:

$$< Q >= \omega\tau. \qquad (4)$$

The chamber time constant is usually extracted from the power delay profile (PDP) which can be measured without knowledge of the antenna radiation efficiency.

The PDP measured in an RC has an exponential form, which is [10]:

$$\mathrm{PDP}_{f_0}(t) = V_s^2 \exp(-\frac{t}{\tau}), \qquad (5)$$

where the subscript f_0 means the centre frequency at which a band-limited PDP is measured; V_s is a constant giving the initial signal level, and its square is proportional to the initial energy stored in the RC. If the PDP is plotted in decibels, it is a straight line whose slope is determined by the value of the chamber time constant [14]:

$$10 \log_{10}\left[\mathrm{PDP}_{f_0}(t)\right] = \left(-\frac{10 \log_{10} e}{\tau} \right) t + 20 \log_{10} V_s. \qquad (6)$$

For example, the PDPs measured in the University of York (UoY) RC are illustrated in Fig. 1. The dashed line has a steeper slope than the solid line, which shows the effect of a human subject in the RC. The PDPs shown in Fig. 1 are obtained from the inverse Fourier transform (IFFT) of the S_{21}
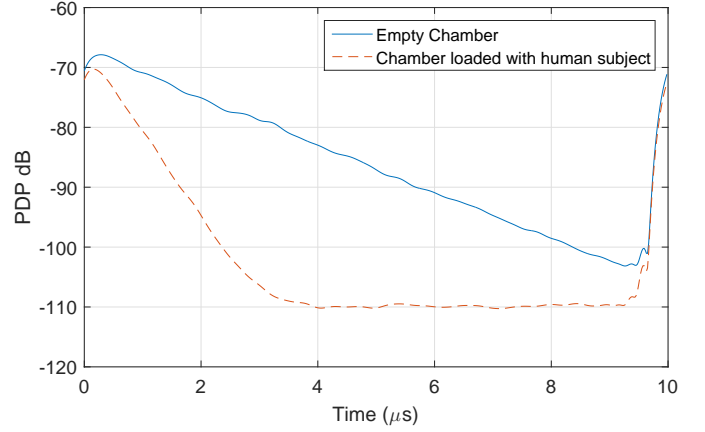

Fig. 1. The PDPs measured in the University of York RC at 10 GHz. Loading a human subject (176 cm height, 70.2 kg weight) in the RC would increase the energy loss speed.
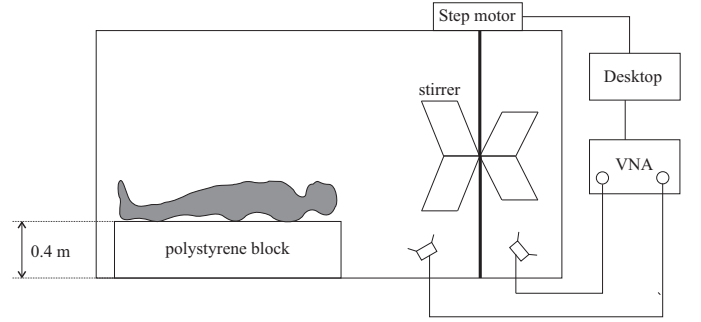

Fig. 2. The setup for human body ACS measurement. The subject lies on a polystyrene block with height 0.4 m, which is greater than one wavelength at 1 GHz

filtered by a window function to select the required frequency range:

$$\mathrm{PDP}_{f_0}(t) =< \left| \mathrm{IFFT}\big(S_{21}(f) \cdot W_{f_0}(f)\big) \right|^2 >, \qquad (7)$$

where W_{f_0} denotes the window function centred on f_0. Here $f_0 = 10\,\mathrm{GHz}$ and $W_{f_0}(f)$ is a 5 MHz wide, raised cosine window [15]. Linear regression could be applied to the curves in Fig. 1 to extract τ, from which the Q factor can be determined and substituted into (2) to get the ACS. In order to get an improved accuracy and speed of measurement we have used the techniques described in [14]. This applies a non-linear fitting techniques to extract the time-constant which removes errors caused by the window function, the finite nature of the transform and the noise floor. Also the segmented sweep described in [14] is used to minimise the measurement time, which is important for human subjects. The segmented sweeping means we only sweep those frequencies which are included in the band-limited IFFT.

A polystyrene block was used to support the human body at least one wavelength above the ground and within the working volume of the RC, where the field is properly uniform, as shown in Fig. 2. This was not always done in the previous research. The 48 human subjects under test (SUT) were asked to hold a specific posture for each measurement, since the ACS of an individual is highly dependent on his or her posture.

B. Validation of the ACS measurement techniques

In order to test the accuracy of the ACS measurement techniques presented in the previous section, we measured the ACS of a sphere model with known material and structure. We choose a sphere because its ACS can be calculated analytically by Mie series. The code of Mie series used in this research is SPlaC v1.01 [16].

The sphere model is a high density polyethlene (HDPE) spherical shell filled with deionized water. The thickness of the shell measured, close to its rim, using a caliper, is 3.9 mm. The relative permittivity of the spherical shell assumed to be 2.35 [17]. The radius of the sphere is 193.6 mm, which is determined from the circumference at the equator. The dielectric properties of the deionized water is calculated using Kaatze's formula [18] with the room temperature equal to $20\,^\circ$C.

The measurement is conducted in the University of York RC, which is a zinc galvanized room of dimension $4.7\,\mathrm{m} \times 3\,\mathrm{m} \times 2.37\,\mathrm{m}$. The measurement set-up is shown in Fig. 3. Segmented frequency sweeping is applied with center frequencies of the segments stepped linearly from 1 GHz to 16 GHz with a step of 100 MHz. Each segments is 5 MHz wide and the frequency points in each segment are 100 kHz apart. It takes 11 minutes to record 800 sweeps during which the stirrer roatates 360°. The ACS is extracted from chamber time constant and the result is shown in Fig. 4. It can be seen that the measurements match very well with the simulation. The mean absolute percentage error (MAPE) of the measurement is less than 3.4%. The MAPE of the measured ACS is defined as:

$$\mathrm{MAPE}(<\sigma_{\mathrm{a,meas}}>) = \\ \mathrm{mean}\left(\left|\frac{<\sigma_{\mathrm{a,meas}}(f)> - <\sigma_{\mathrm{a,Mie}}(f)>}{<\sigma_{\mathrm{a,Mie}}(f)>}\right|\right) \times 100\%, \quad (8)$$

where $<\sigma_{\mathrm{a,meas}}(f)>$ is the measured ACS at frequency f; $<\sigma_{\mathrm{a,Mie}}(f)>$ is the ACS calculated by Mie series at frequency f; $\mathrm{mean}(\cdot)$ denotes averaging over all frequencies.

As a comparison, the ACS of the sphere is also determined by (3) with the same measurement set-up. Since the application of (3) requires antenna radiation efficiency to be known, both the values of η_{tx} and η_{rx} were set to 0.9 firstly, and then to 1.0. In our experience, the radiation efficiencies of horn-like antennas typically range form 0.9 to 1.0. The ACS results given by (3) is plotted in Fig. 5. The MAPE of measured ACS is 35.3% for $\eta_{\mathrm{Tx}} = \eta_{\mathrm{Tx}} = 1.0$; 12.9% for $\eta_{\mathrm{Tx}} = \eta_{\mathrm{Tx}} = 0.9$. Both of them are larger than the MAPE of the ACS determined by IFFT techniques. Even though the multiplication of η_{Tx} and η_{Rx} can be solved by inserting (4) to the left side of (3), this approach is pointless in comparing (3) and (4), because substituting the obtained antenna efficiencies back into (3) will produce exactly the same Q factor as (4) does.

This validation experiment demonstrates the accuracy of the measurement techniques, and we would use the same techniques to measure the ACS of human body.

Fig. 3. The set-up for measuring the sphere model in the University of York RC. The transmitting antenna (ETS 3117) and receiving antenna (ETS 3115) are cross polarized and pointed away from each other to reduce the direct coupling.
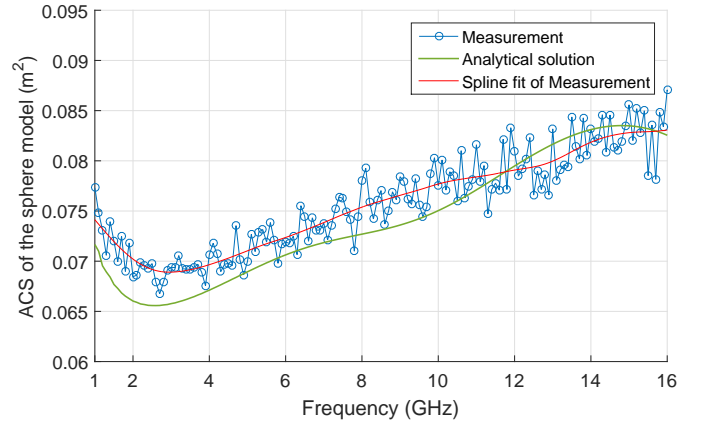

Fig. 4. The ACS of the sphere model determined from the chamber time constant compared to the analytical solution calculated by Mie series. A spline curve is fitted to the measuremed result for easy comparison with the analytical solution. De Bour's approach is applied in the spline fit, with smoothing factor of 0.5 [19].
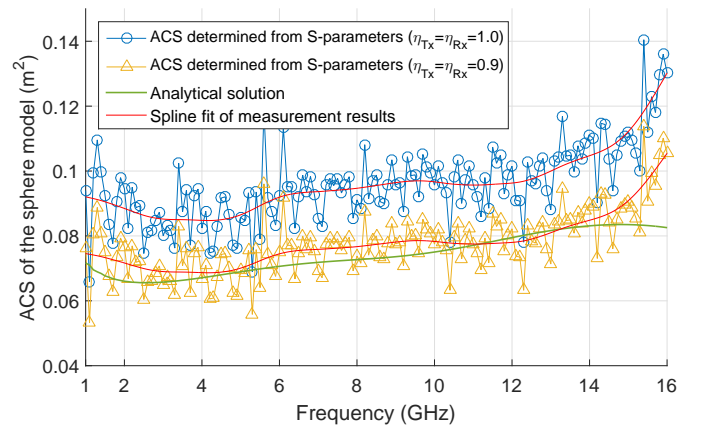

Fig. 5. The ACS of the sphere model determined directly from S-parameters in the frequency domain.

TABLE I
THE AVERAGE FACTOR BY WHICH THE HUMAN BODY ACS IS CHANGED
DUE TO THE CHANGE OF POSTURES OVER THE FREQUENCY RANGE 1 GHz
TO 16 GHz (RELATIVE TO THE ACS OF SUPINE-B)

Posture	Male	Female
Sitting-A	0.87	0.85
Sitting-B	0.95	0.92
Supine-A	0.97	0.95
Supine-B	1.00	1.00
Supine-C	1.02	1.01

C. Effect of posture on the human body ACS

Previous studies have shown that the posture of human body can change its ACS a lot. The numerical simulation conducted by Uusitupa et al. shows a seated posture could decrease the whole body specific absorption rate (SAR) by 10% comparing to a standing posture [20].

In this section, a preliminary measurement was performed to study the posture's effect on the human body ACS. The measurement setup is the same as that given in Fig. 2. A male and a female subject were put under test. The male subject is of 180 cm height, 84.5 kg weight. The female subject is of 166 cm height, 55.3 kg weight. The five different postures under test are shown in Fig. 6. The measurement result is illustrated in Fig. 7 and Fig 8.

Fig. 7 and Fig. 8 show that for both subjects, the ACS curves of five different postures do not have apparent differences in shape, but different in the overall level. The reason for ACS change could be the shadowing effect of limbs. For instance, in the 'Sitting-A' posture, the upper arms of the subject block the illumination of EM waves on the side of rib cage; Switching from 'Sitting-A' to 'Sitting-B' by rising arms allows better exposure of rib cage in the EM field, thus an observable change on the ACS is induced. The figures also show that more stretched postures tend to have higher ACS in diffuse environments. We choose 'Supine-B' for all the subjects in the group study, because it gives high exposure in the fields and it is relatively comfortable to hold during the measurement.

Fig. 7 and Fig. 8 suggest that the posture tends to change the human body ACS by a certain factor which is almost constant from 1 GHz to 16 GHz. In order to obtain such a factor, the ACS values of different postures are divided by the ACS of 'Supine-B', then averaged from 1 GHz to 16 GHz. The results are given in Table. I. These results could be helpful in evaluating the ACS of human body in different postures.

D. The measurement of morphological parameters

The following three morphological parameters are measured in the study: height, weight, and averaged skin fold thickness; The body mass index (BMI), body fat percentage (BFP), and body surface area (BSA) are evaluated from the measured morphological parameters using empirical formulas.

The height is measured using a tape-measure, and body mass is measured by an electronic scale. The skin fold thickness is measured with a slim guide caliper [21]. The caliper has springs fixed on the jaws to maintain a constant pressure during the measurement. The skin fold measurements were performed at four positions: the triceps, the abdominal wall,
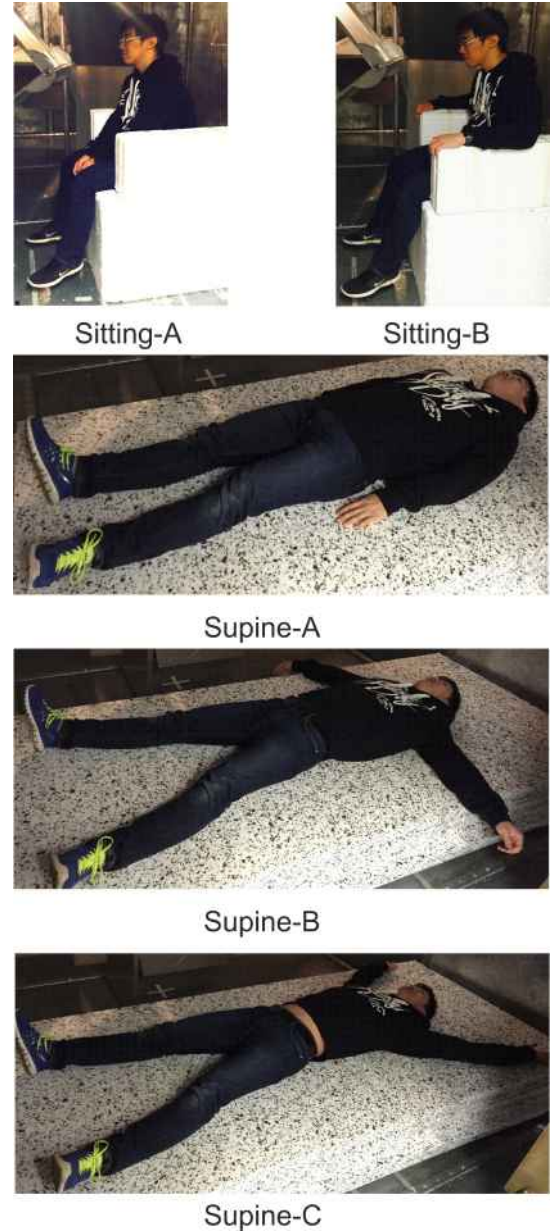

Fig. 6. The human body positions under study. 1) Sitting-A: Regular sitting pose with arms rest between the thighs; 2) Sitting-B: Regular sitting pose with arms on the armrest; 3) Supine-A: Regular supine position; 4) Supine-B: Supine position with hands far away from the midline. 5) Supine-C: Supine position with arms raised over the subject's head.

the thigh and the suprailiac crest. The skin fold measurement was performed according to the International Standards of Anthropometic Assessment and each measurement is repeated three times [21]. The averaged skin fold thickness is taken by averaging the twelve measurements.

The BFP is calculated from the summation of the skin fold thicknesses using the 4-site formula [22], [23]:

$$\mathrm{BFP} = 0.29288 \sum d_{\mathrm{sf}} - 0.0005 \left(\sum d_{\mathrm{sf}} \right)^2 +$$
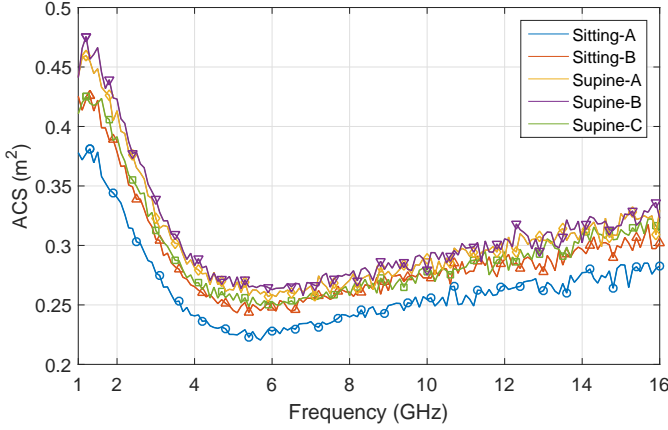$$0.15845Y - 5.76377 \quad (\mathrm{for\ male}) \ , \quad (9)$$

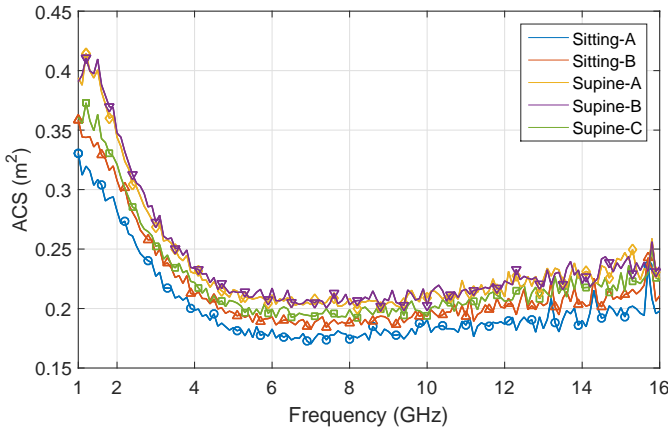Fig. 7. The measured ACS of a male subject with different body positions

Fig. 8. The measured ACS of a female subject with different body positions

$$\text{BFP} = 0.29669 \sum d_{\text{sf}} - 0.00043 \left(\sum d_{\text{sf}}\right)^2 +$$
$$0.02963Y + 1.4072 \quad (\text{for female}) , \quad (10)$$

where $\sum d_{\text{sf}}$ is the summation of the the skin fold reading at the four sites in mm; Y is age in years.

The BSA is evaluated from the height and weight using the Tikuisis formula [24]:

$$\begin{cases} \text{BSA} = 128.1 m^{0.44} h^{0.60} \ (\text{for men}) \\ \text{BSA} = 147.4 m^{0.47} h^{0.55} \ (\text{for women}) \end{cases} , \quad (11)$$

where BSA is in cm^2; m is body mass in kg; h is height in cm. The overall relative root mean square (RMS) error of (11) is 1.26% [24].

III. GROUP STUDY AND DISCUSSION

The 48 human SUTs were recruited from the faculty members and students in the Department of Electronic Engineering, at the University of York. An overview of their morphological parameters is in Table II and Table III.

The position of SUT and antennas is shown in Fig. 2. The measurement procedure is the same as that in the validation experiment presented in Section II-B. In order to

TABLE II
THE MORPHOLOGICAL PARAMETERS OF THE 33 MALE SUBJECTS

	range	mean	median
Age (Years)	19-58	27	24
Height (cm)	160-190	177	176
Weight (kg)	52.6-142.4	77.0	74.8
Averaged skin fold thickness (mm)	6.4-52.2	18.8	19.4
BSA (m^2)	1.6-2.5	1.9	1.9
BMI (kg $\cdot$ m^{-2})	18.4-47.0	24.7	24.6
BFP (skin-fold method %)	4.9-37.0	14.8	15.2

TABLE III
THE MORPHOLOGICAL PARAMETERS OF THE 15 FEMALE SUBJECTS

	range	mean	median
Age (Years)	19-55	27	24
Height (cm)	158-169	164	166
Weight (kg)	43.5-72.3	56.3	55.1
Averaged skin fold thickness (mm)	11.3-35.2	19.0	17.7
BSA (m^2)	1.4-1.8	1.62	1.62
BMI (kg $\cdot$ m^{-2})	17.0-26.9	20.8	20.3
BFP (skin-fold method %)	14.7-35.1	22.9	23.1

verify the effectiveness of the human body ACS measurement, the measured ACS values of four SUTs are compared to the documented ACS values of four human voxel models with similar morphological parameters (NORMAN, NAOMI, TARO, HANAKO) [25], [26], [27]. Even though we endeavoured to look for female SUTs that are of more similar BFP to the voxel models than the current two SUTs, no such female SUTs were found because their height and weight are very different to the voxel models. The current two female SUTs are selected to maximize the plausibility of the comparison within the scope of this research. All the morphological parameters, including those of the voxel models and those of the SUTs, are compared in Table IV. In the table, the morphological parameters of the subjects are given in the column labelled by 'SUT', and the subscript of 'SUT' gives the name of the voxel model that has similar morphological parameters to that subject. It is important to point out that the documented ACS values of these voxel models are not calculated in a diffuse environment, but with a plane wave incident on the front of the model, with the direction of E-field parallel to the model's midline. According to the research of Flintoft, the ACS values of voxel models calculated in this case should still be comparable to the ACS values measured in diffuse environments, if the ACS in diffuse environment is increased by a certain factor [28]. In Fig. 10, the measured ACS values of the four SUTs are all increased by a factor of 1.3, and they all match well with the ACS values of the corresponding voxel models. This factor 1.3 is slightly smaller than the range 1.4-1.6 given by Flintoft, because the postures of subjects under test in Flintoft's research is 'Sitting-A', while in ours is 'Supine-B', as shown in Fig. 4. The RMS differences between the ACS values of SUTs and the ACS values of corresponding voxel models are: 0.05 m^2 for NORMAN, 0.03 m^2 for NAOMI, 0.01 m^2 for TARO, 0.02 m^2 for HANAKO.

The correlation coefficients between the measured ACS values and morphological parameters are calculated from 1 GHz to 16 GHz, and the results are illustrated in Fig. 11. The figure shows that above 6 GHz, the BSA has the highest correlation

TABLE IV
THE MORPHOLOGICAL PARAMETERS OF VOXEL MODELS AND
CORRESPONDING SUBJECTS UNDER TEST

	NORMAN	SUT$_{\text{NORMAN}}$	NAOMI	SUT$_{\text{NAOMI}}$
Height (cm)	176	176	163	163
Weight (kg)	73.01	72.2	59.88	60.7
BFP (%)	22	15	40	27
	TARO	SUT$_{\text{TARO}}$	HANAKO	SUT$_{\text{HANAKO}}$
Height (cm)	173	173	160	161
Weight (kg)	65	69.7	53	53.3
BFP (%)	22	18	31	23

coefficient to the measured ACS among all morphological parameters, which can be explained by the low penetration depth of EM wave into human tissues at high frequencies. For instance, the penetration depth for dry skin is less then 1 cm above 6 GHz [5].

Due to the strong correlation between the BSA and the human body ACS, an empirical formula can be obtained by linear regression:

$$< \sigma_{a,eval}(f) > = C_1(f) \times \text{BSA} + C_2(f) \quad (12)$$

where $< \sigma_{a, eval}(f) >$ denotes the evaluated human body ACS in diffuse environments in m^2; BSA is calculated by (11) and converted into m^2 in this formula; $C_1(f)$ and $C_2(f)$ are two coefficients that vary with frequency.

$C_1(f)$ and $C_2(f)$ are plotted in Fig. 12. The figure shows the value of $C_2(f)$ is very close to zero above 6 GHz, which means the BSA is almost the only factor that dominates the ACS. However, below 6 GHz, $C_2(f)$ is not zero, which means ACS might be determined by some other factors as well as the BSA.

For the easy application of (12), the coefficients $C_1(f)$ and $C_2(f)$ are fitted to polynomials, and the results are:

$$\begin{cases} C_1(f) = -0.00278f^3 + 0.03995f^2 - 0.16958f + 0.28820 \\ C_2(f) = 0.00465f^3 - 0.05927f^2 + 0.19557f - 0.02444 \\ f \in [1\,\text{GHz}, 6\,\text{GHz}] \end{cases}$$

$$\begin{cases} C_1(f) = 0.00006f^3 - 0.00274f^2 + 0.03979f - 0.04430 \\ C_2(f) = -0.00013f^3 + 0.00554f^2 - 0.07335f + 0.28879 \\ f \in (6\,\text{GHz}, 18\,\text{GHz}] \end{cases}$$

$$(13)$$

where f is frequency in GHz. Since the curve of $C_1(f)$ has a greater variation below 6 GHz than it does above 6 GHz, the polynomial fitting of $C_1(f)$ are performed below and over 6 GHz independently. $C_2(f)$ is fitted in the same way for the same reason. The results of polynomial fitting are also shown in Fig. 12.

The goodness of the polynomial fitting is tested by substituting (13) back into (12) to evaluate the ACS values of the 48 subjects, and then calculate the MAPE of the evaluated ACS relative to the measurement result. The MAPE of the evaluated ACS of 48 sujects are plotted as the cumulative distribution function (CDF) in Fig. 9. It shows that (12) gives ACS within 6% MAPE for 80% of the subject from 1 GHz to 16 GHz.
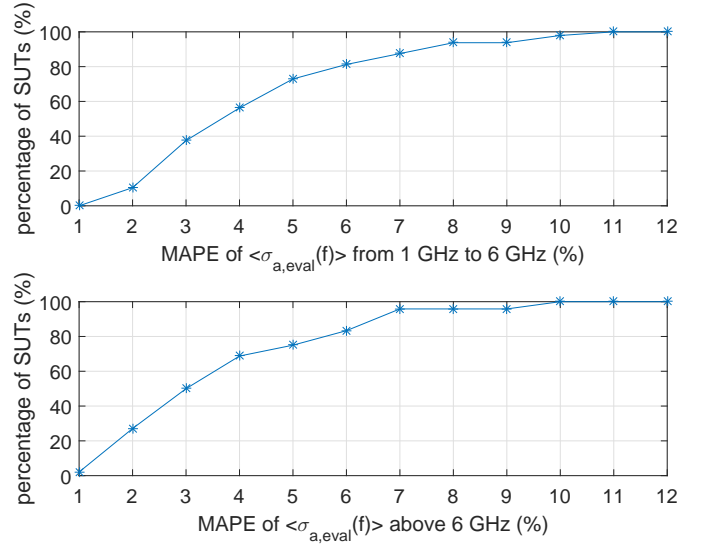

Fig. 9. The MAPE($< \sigma_{a,eval}(f) >$) plotted as cumulative distribution function (CDF). The formula of $< \sigma_{a,eval}(f) >$ is given in (12).
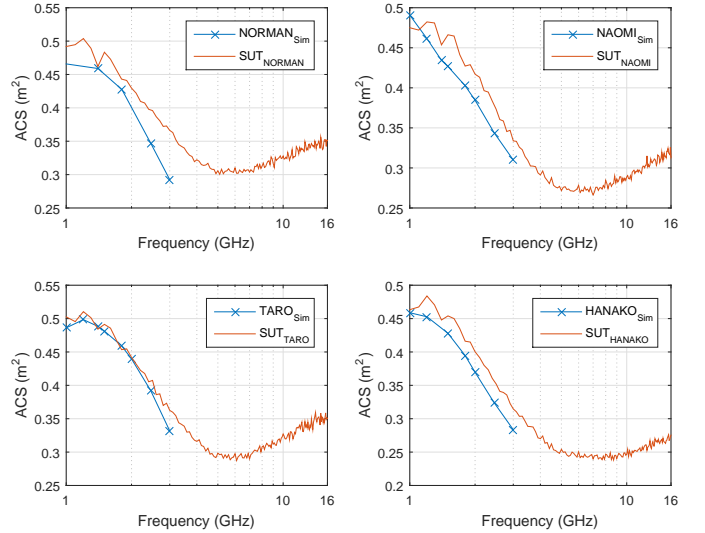

Fig. 10. Comparison between the measured human body ACS and documented simulations results in [27]. The measured ACS values are all increased by a factor of 1.3. In the legends, 'Name of Voxel Model$_{\text{Sim}}$' denotes documented simulation result of the voxel model; 'SUT$_{\text{Name of Voxel Model}}$' is the measured ACS of the SUT who has similar morphological parameters to the corresponding voxel model.

IV. CONCLUSIONS

In order to give an empirical formula for the human body ACS in diffuse environment, the ACS of 48 human subjects was measured in an RC from 1 GHz to 16 GHz. The measurement techniques were verified by measuring the ACS of a sphere model with known structure and material, and the MAPE of the measurement result is only 3.4% relative to the numerical calculation. The measurement technique was applied in the preliminary study on effect of postures on the human body ACS. The posture study shows the ACS values of supine postures are at least 10% higher than the ACS values of seating poses. Strong linear correlations were found between BSA and ACS from 1 GHz to 16 GHz. Especially over 6 GHz,
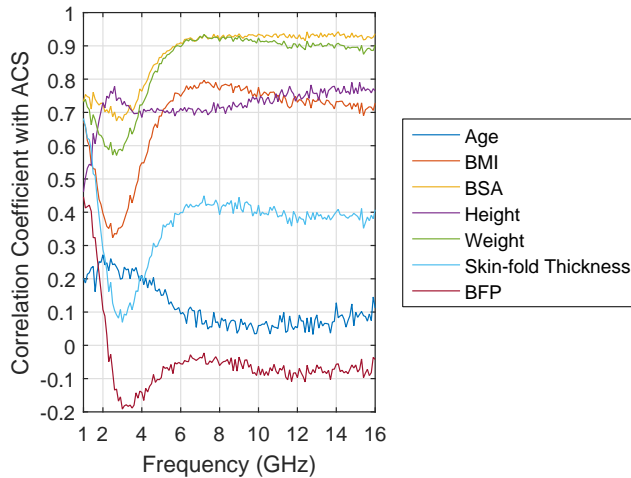
Fig. 11. Correlation coefficients between the human body ACS and morphological parameters from 1 GHz to 16 GHz. The 'Skin-fold thickness' denotes averaged skin fold thickness; 'BFP' is calculated using formula (9) and (10)
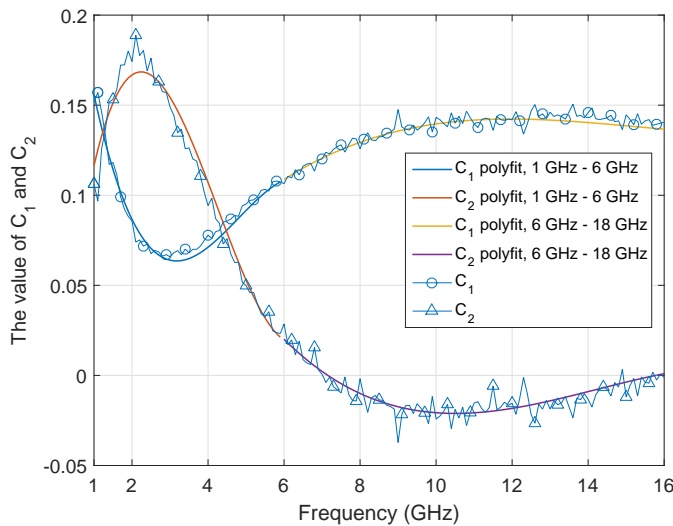

Fig. 12. C_1 and C_2 value over different frequencies

the correlation coefficients between ACS and BSA stays over 0.9. The correlation between the ACS and BFP is not clear. Therefore the empirical formula of human body ACS is written as a linear function of BSA from 1 GHz to 16 GHz. The empirical formula fits well with the measurement data. For more than 80% of the SUTs, the empircial formula gives the ACS with less than 6% of MAPE relative to the corresponding measurement results.

ACKNOWLEDGMENT

REFERENCES

[1] J. Andersen, K. L. Chee, M. Jacob, G. Pedersen, and T. Kurner, "Reverberation and absorption in an aircraft cabin with the impact of passengers," *IEEE Transactions on Antennas and Propagation*, vol. 60, no. 5, pp. 2472–2480, May 2012.

[2] A. Bamba, D. Gaillot, E. Tanghe, G. Vermeeren, W. Joseph, M. Lienard, and L. Martens, "Assessing whole-body absorption cross section for diffuse exposure from reverberation chamber measurements," *IEEE Transactions on Electromagnetic Compatibility*, vol. 57, no. 1, pp. 27–34, Feb 2015.

[3] G. C. R. Melia, M. P. Robinson, I. D. Flintoft, A. C. Marvin, and J. F. Dawson, "Broadband measurement of absorption cross section of the human body in a reverberation chamber," *Electromagnetic Compatibility, IEEE Transactions on*, vol. 55, no. 6, pp. 1043–1050, 2013.

[4] E. Genender, C. L. Holloway, K. A. Remley, J. M. Ladbury, G. Koepke, and H. Garbe, "Simulating the multipath channel with a reverberation chamber: Application to bit error rate measurements," *IEEE Transactions on Electromagnetic Compatibility*, vol. 52, no. 4, pp. 766–777, Nov 2010.

[5] G. C. R. Melia, "Electromagnetic Absorption by the human body from 1 to 15 GHz," Ph.D. dissertation, Department of Electronic, The University of York, 2013.

[6] C. L. Holloway, H. A. Shah, R. J. Pirkl, W. F. Young, D. A. Hill, and J. Ladbury, "Reverberation chamber techniques for determining the radiation and total efficiency of antennas," *IEEE Transactions on Antennas and Propagation*, vol. 60, no. 4, pp. 1758–1770, 2012.

[7] D. Senić, A. Sarolić, Z. M. Jóskiewicz, and C. L. Holloway, "Absorption cross-section measurements of a human model in a reverberation chamber," *IEEE Transactions on Electromagnetic Compatibility*, vol. 58, no. 3, pp. 721–728, June 2016.

[8] D. Senić, "Human exposure and wireless communication aspects of electromagnetic wave absorption in dissipative objects inside reverberant environments," Ph.D. dissertation, Faculty of electronic engineering, mechanical engineering and naval architecture, The University of Split, 2014.

[9] Z. Tian, Y. Huang, Q. Xu, T. H. Loh, and C. Li, "Measurement of absorption cross section of a lossy object in reverberation chamber without the need for calibration," in *2016 Loughborough Antennas Propagation Conference (LAPC)*, Nov 2016, pp. 1–5.

[10] D. A. Hill, *Electromagnetic fields in cavities: deterministic and statistical theories*. New York: John Wiley & Sons, 2009.

[11] D. Hill, M. T. Ma, A. R. Ondrejka, B. F. Riddle, M. L. Crawford, R. T. Johnk *et al.*, "Aperture excitation of electrically large, lossy cavities," *Electromagnetic Compatibility, IEEE Transactions on*, vol. 36, no. 3, pp. 169–178, 1994.

[12] I. D. Flintoft, G. C. Melia, M. P. Robinson, J. F. Dawson, and A. C. Marvin, "Rapid and accurate broadband absorption cross-section measurement of human bodies in a reverberation chamber," *Measurement Science and Technology*, vol. 26, no. 6 065701, 2015.

[13] U. Carlberg, P.-S. Kildal, A. Wolfgang, O. Sotoudeh, and C. Orlenius, "Calculated and measured absorption cross sections of lossy objects in reverberation chamber," *IEEE Transactions on Electromagnetic Compatibility*, vol. 46, no. 2, pp. 146–154, 2004.

[14] X. Zhang, M. P. Robinson, I. D. Flintoft, and J. F. Dawson, "Efficient determination of reverberation chamber time constant," *IEEE Transactions on Electromagnetic Compatibility*, vol. 60, no. 5, pp. 1296–1303, Oct 2018.

[15] I. Glover and P. M. Grant, *Digital communications*. Essex, England: Pearson Education, 2010.

[16] E. Le Ru and P. Etchegoin, "SPlaC package v1.0 guide and supplementary information," Victoria University, Tech. Rep., 2008. [Online]. Available: http://www.victoria.ac.nz/scps/research/research-groups/raman-lab/numerical-tools/sers-and-plasmonics-codes

[17] B. Riddle, J. Baker-Jarvis, and J. Krupka, "Complex permittivity measurements of common plastics over variable temperatures," *IEEE Transactions on Microwave Theory and Techniques*, vol. 51, no. 3, pp. 727–733, 2003.

[18] U. Kaatze, "Complex permittivity of water as a function of frequency and temperature," *Journal of Chemical and Engineering Data*, vol. 34, no. 4, pp. 371–374, 1989.

[19] C. D. Bour, *A practical guide to splines*. New York: Splinger-Verlag, 2001.

[20] T. Uusitupa, I. Laakso, S. Ilvonen, and K. Nikoskinen, "SAR variation study from 300 to 5000 MHz for 15 voxel models including different postures," *Physics in medicine and biology*, vol. 55, no. 4, p. 1157, 2010.

[21] International Society for the Advancement of Kinanthropometry, "International Standards for Anthropometric Assessment," 2001.

[22] C. Balasubramaniana and B. Chittibabub, "Effect of handball specific aerobic training on body composition and VO2 max of male handball players," *International Journal of Physical Education, Fitness and Sports*, pp. 3–4, 2014.

[23] M. Leslie and C. Mikanowicz, "Assessment of body composition in the healthy adult," *Journal of the American Association of Nurse Practitioners*, vol. 9, no. 3, pp. 123–127, 1997.

[24] P. Tikuisis, P. Meunier, and C. Jubenville, "Human body surface area: measurement and prediction using three dimensional body scans," *European journal of applied physiology*, vol. 85, no. 3, pp. 264–271, 2001.

[25] P. Dimbylow, "FDTD calculations of the whole-body averaged SAR in an anatomically realistic voxel model of the human body from 1 MHz to 1 GHz," *Physics in Medicine & Biology*, vol. 42, no. 3, p. 479, 1997.

[26] ——, "Development of the female voxel phantom, NAOMI, and its application to calculations of induced current densities and electric fields from applied low frequency magnetic and electric fields," *Physics in Medicine & Biology*, vol. 50, no. 6, p. 1047, 2005.

[27] P. J. Dimbylow, A. Hirata, and T. Nagaoka, "Intercomparison of whole-body averaged SAR in European and Japanese voxel phantoms," *Physics in Medicine & Biology*, vol. 53, no. 20, p. 5883, 2008.

[28] I. Flintoft, M. Robinson, G. Melia, A. Marvin, and J. Dawson, "Average absorption cross-section of the human body measured at 1–12 GHz in a reverberant chamber: results of a human volunteer study," *Physics in Medicine and Biology*, vol. 59, no. 13, p. 3297, 2014.